RSC Advances

PAPER

Cite this: *RSC Adv.*, 2022, **12**, 860

Effect of surface properties of TiO_2 on the performance of Pt/TiO_2 catalysts for furfural hydrogenation†

Mi Yeon Byun,[ab] Ye Eun Kim,[ad] Jae Ho Baek,[a] Jungho Jae*[c] and Man Sig Lee*[ae]

Received 28th September 2021
Accepted 10th December 2021

DOI: 10.1039/d1ra07220j

rsc.li/rsc-advances

Hydrogenation of biomass-derived furfural is an important process in biofuel production. Herein, different Pt-supported TiO_2 morphologies: nanorod (NR), nanoparticle (NP), and hollow microsphere (HMS) were prepared by the impregnation–chemical reduction method. The furfural conversion increased with an increase of Pt dispersion. However, cyclopentanone selectivity was affected by TiO_2 properties, the strong metal–support interaction (SMSI) effect, and the reaction conditions. The Pt/TiO_2 NR catalyst exhibited the highest cyclopentanone selectivity of 50.4%. Based on the H_2-temperature programmed desorption (H_2-TPD) and X-ray photoelectron spectroscopy (XPS) results, the Pt/TiO_2 NR catalyst showed a SMSI effect, which was introduced by the chemical reduction method. We suggest that electron charge transfer from Ti species to Pt in the Pt/TiO_2 NR catalyst affects the cyclopentanone selectivity by controlling the adsorption strength between the reactant and the Pt surface, thus retarding the formation of byproducts.

1. Introduction

TiO_2 is widely used in the chemical industry as a semiconductor, photocatalyst, and catalyst support owing to its unique properties.[1] TiO_2 has various advantages as a catalyst support, including chemical stability, acid–base properties, and strong metal–support interactions (SMSIs). Recently, various types of TiO_2 with zero-dimensional (0D, nanoparticles (NPs)), one-dimensional (1D, nanowires, nanorods (NRs), and nanobelts), two-dimensional (2D, nanosheets), and three-dimensional structures (3D, hollow microspheres (HMSs)) have been applied as catalysts or catalyst supports. Tian *et al.* reported that Pd/TiO_2 nanowires exhibited higher catalytic activity than Pd/TiO_2 (P25) in the selective hydrogenation of phenolics to cyclohexanones,[2] as Lewis acid and basic sites exposed on the TiO_2 surface improved the cyclohexanone selectivity. Song *et al.* reported the selective oxidation of benzyl alcohol to benzaldehyde over a Pt/TiO_2 nanosphere catalyst.[3] In this system, the hollow TiO_2 structure enhanced the diffusion and infiltration of reactants. Alqurashi *et al.* reported that TiO_2 NPs contributed to the formation of small and uniform Fe_2O_3 NPs, resulting in high activity for benzyl alcohol oxidation.[4] The performance of a catalyst is strongly affected by the support properties, such as acid–base properties, specific surface area, oxygen vacancies, and porosity.

With the depletion of fossil fuels, alternative energies have received considerable attention. Furfural derived from biomass resources is considered an important starting material for the production of valuable chemical products such as furfuryl alcohol (FA), tetrahydrofurfuryl alcohol (THFAL), tetrahydrofuran (THF), 2-methylfuran (2-MF), and cyclopentanone (CPO) by hydrogenation or rearrangement. These materials are mostly used for manufacturing biofuel, bioplastics, and pharmaceuticals. In particular, the selective rearrangement of furfural to CPO has attracted attention because CPO is widely used in the pharmaceutical, food and chemical industries. Various supported catalysts, such as Pd/TiO_2, Pd–Cu/C, Pt/C, and Ru/C, have been used in hydrogenation reactions.[5–8] However, few studies have investigated on the effect of TiO_2 properties on the catalytic performance of Pt/TiO_2 catalysts for furfural hydrogenation. Herein, we prepared Pt-supported TiO_2 catalysts (NR, NP, and HMS supports) by impregnation and chemical reduction. The catalytic activities were determined using the aqueous phase hydrogenation of furfural to CPO. Furthermore, the contribution of the strong metal-support interaction (SMSI) effect to the activity and selectivity of the Pt/TiO_2 catalysts for furfural hydrogenation was investigated.

[a]*Ulsan Division, Korea Institute of Industrial Technology (KITECH), Ulsan 44413, Republic of Korea. E-mail: lms5440@kitech.re.kr*

[b]*Department of Polymer Science and Chemical Engineering, Pusan National University, Busan 46241, Republic of Korea*

[c]*School of Chemical Engineering, Pusan National University, Busan 46241, Republic of Korea. E-mail: jh.jae@pusan.ac.kr*

[d]*Department of Chemical and Biological Engineering, Korea University, Seoul 02841, Republic of Korea*

[e]*Department of Green Process and System Engineering, University of Science and Technology (UST), Ulsan 44413, Republic of Korea*

† Electronic supplementary information (ESI) available. See DOI: 10.1039/d1ra07220j

2. Experimental

2.1. Synthesis of TiO_2 supports

2.1.1. TiO_2 NR. The TiO_2 NR were prepared using a titanium glycolate precursor.[9,10] Typically, 1.75 g of titanium(IV) butoxide (97%, Sigma-Aldrich) was added to 200 mL of ethylene glycol (99%, Alfa Aesar). The solution was stirred at 30 °C for 1 h. The solution was heated to 150 °C and then stirred for 14 h. The suspension was then filtered, washed with ethanol and deionized water for several times, and then dried at 105 °C for 24 h in an oven.

2.1.2. TiO_2 NP. The TiO_2 NP were prepared using a titanium glycolate precursor with acetone.[11] Typically, 5.0 g of titanium(IV) butoxide was added to 50 mL of ethylene glycol. The solution was vigorously stirred at 25 °C for 24 h. Then, 340 mL of acetone and 2.7 mL of deionized water were added and vigorously stirred at 25 °C for 1 h 30 min. The suspension was centrifuged and washed with ethanol and deionized water, and then dried at 105 °C overnight in an oven. Subsequently, 1.0 g of the prepared white powder was added to 200 mL of deionized water and then heated to 90 °C for 1 h under stirring. The suspension was filtered, washed with ethanol and deionized water, and dried at 105 °C for 24 h in an oven.

2.1.3. TiO_2 HMS. The TiO_2 HMS were prepared by a template-free solvothermal method.[3] Typically, 16 g of oxalic acid (98%, Sigma-Aldrich) was added to 50 mL of ethanol, and then the suspension was vigorously stirred at 25 °C for 10 min. Then, 2.0 g of titanium(IV) butoxide was quickly added and vigorously stirred at 25 °C for 10 min. The mixture was transferred to a 100 mL hydrothermal reactor, which was heated to 140 °C for 12 h in an oven. The suspension was filtered, washed with ethanol and deionized water, and dried at 105 °C for 24 h in an oven. All the TiO_2 supports were calcined at 500 °C (heating rate = 5 °C min^{-1}) for 2 h under flowing air.

2.2. Preparation of Pt/TiO_2 catalysts

5wt% Pt/TiO_2 catalysts were prepared by the impregnation–chemical reduction method. Briefly, the $H_2PtCl_6 \cdot 6H_2O$ (37.5%, Wako Pure Chemical Cooperation) was added to 50 mL of deionized water. Then, 0.65 g of TiO_2 support was added and stirred at 25 °C for 1 h. The Pt/TiO_2 catalysts were reduced in the liquid phase using 5 mL of $NaBH_4$ (0.15 M, 99%, Sigma-Aldrich) solution. The suspension was stirred at 25 °C for 12 h and then filtered, washed with deionized water, and dried at 105 °C for 24 h in an oven.

2.3. Characterization

Specific surface area, pore diameters and volumes were calculated by Brunauer–Emmett–Teller (BET) and Barrett–Joyner–Halenda (BJH) analyses of N_2 isotherm curves at 77 K using a Micromeritics ASAP 2020 instrument. The X-ray diffraction (XRD) analysis was carried out on a Bruker D8 Focus instrument using a Cu Kα radiation. The temperature-programmed reduction of H_2 (H_2-TPR) and temperature-programmed desorption of H_2 or NH_3 (H_2-TPD or NH_3-TPD) were carried out using a Micromeritics AutoChem 2920 instrument equipped with a TCD detector. In the H_2-TPR analysis, 100 mg of catalyst was pre-treated under a continuous He flow at 150 °C for 2 h. The catalyst was heated to 750 °C (heating rate = 10 °C min^{-1}) under a H_2 (5% H_2 in He balance) flow. In the H_2-TPD analysis, 50 mg of catalyst was pre-treated under H_2 (10% H_2/Ar) flow at 400 °C for 1 h. Then, the catalyst was cooled into ambient temperature and heated to 800 °C (heating rate = rate = 10 °C min^{-1}) under a He flow. In the NH_3-TPD analysis, 100 mg of catalyst was pre-treated under He flow at 150 °C for 2 h. Subsequently, NH_3 (10% NH_3 in He balance) adsorption was carried out at 50 °C for 0.5 h. The catalysts were heated to 600 °C (heating rate = 10 °C min^{-1}) under a constant He flow. X-ray photoelectron spectroscopy (XPS) was carried out using a Thermo Fisher Scientific K Alpha+ instrument with Al Kα radiation. The surface morphologies of the supports were determined by scanning electron microscopy (SEM) on a Hitachi SU8020 instrument operated at 15 kV. Pt dispersion was estimated by CO pulse chemisorption using a Micromeritics AutoChem 2920 instrument. The average particle size and distribution of Pt in Pt/TiO_2 catalysts were measured by field-emission transmission electron microscopy (FE-TEM) using a JEOL JEM-2100F instrument operating at 200 kV.

2.4. Furfural hydrogenation

Furfural hydrogenation was conducted in a 250 mL batch reactor using 0.1 g of Pt/TiO_2 catalyst, and 100 mL of deionized water containing 2.5 g of furfural. After rapidly transferring the mixture into the reactor, the reactor was sealed and introduced with hydrogen three times to remove air. After reaching the desired temperature, reactor was pressurized with hydrogen 20 bar under stirring at 500 rpm. The liquid product was analyzed by gas chromatography (7890A, Agilent, FID) with a DB-Wax column (30 m × 0.32 mm × 0.25 μm).[7]

3. Results and discussion

3.1. Characterization of supports and Pt catalysts

Fig. 1 shows the N_2 isotherm curves and pore size distributions of the TiO_2 supports and Pt/TiO_2 catalysts. All the TiO_2 supports had type IV of N_2 adsorption–desorption isotherms. TiO_2 NP exhibited a H1 hysteresis loop, which is indicative of a mesoporous material according to the IUPAC classification. In contrast, TiO_2 NR and TiO_2 HMS showed a hysteresis loop of type H2 (b) type with an ink bottle pore structure. The total pore volumes were calculated by adsorption isotherms at $P/P_0 \sim 0.995$. Capillary condensation in the TiO_2 NP and TiO_2 HMS supports was initiated at a relative pressure (P/P_0) of ~0.48, whereas that in the TiO_2 NR support occurred at a relative pressure of 0.6, which can be attributed to a larger pore size.[12] After Pt loading, the Pt/TiO_2 catalysts exhibited similar characteristics. The physical properties of the TiO_2 supports and Pt/TiO_2 catalysts are listed in Table 1. The TiO_2 NP support has the largest BET surface area and pore volume (56 m^2 g^{-1} and 0.16 cm^3 g^{-1}, respectively), whereas the TiO_2 NR support has the lowest specific surface area and pore volume (10 m^2 g^{-1} and 0.04 cm^3 g^{-1}, respectively). However, the TiO_2 NR support has

the largest pore diameter, which is in agreement with the above-mentioned results.

After Pt loading, the BET surface area and pore volume decreased, which indicates that Pt NPs block the pores for the Pt/TiO_2 NP. Despite of decrease in the BET surface area, the pore volume and pore diameter was slightly increase for the Pt/TiO_2 HMS. It was inferred that the addition of NaOH may filled the pores of TiO_2, which reduces the pore volume and pore size.[13]

Fig. 2 shows the XRD patterns of the TiO_2 supports and Pt/TiO_2 catalysts. The TiO_2 NR and TiO_2 HMS supports exhibited mixtures of anatase (31% and 79%, respectively) and rutile phases (69% and 21%, respectively). In contrast, the TiO_2 NP support exhibited only the anatase phase. The amounts of anatase and rutile phases were calculated using eqn (1) and are listed in Table 1.[14]

$$A\ (\%) = 100/(1 + 1.265(I_R/I_A)) \quad (1)$$

where I_A is the intensity of the anatase peak ($2\theta = 25.3°$) and I_R is the intensity of the rutile peak ($2\theta = 27.4°$). After Pt loading, the XRD patterns of all the Pt/TiO_2 catalysts exhibited a characteristic Pt peak at 40° (Fig. 1), which corresponded to the (111) crystal face of Pt. However, the relative amounts of anatase and rutile phases for each type of support were similar before and after Pt loading.

The acid properties of the TiO_2 supports and Pt/TiO_2 catalysts were estimated by NH_3-TPD, as shown in Fig. 3 and Table 1. The acidities of the supports and catalysts play an important role in the formation of CPO during furfural hydrogenation. Desorption peaks around 50–200, 200–500, and >500 °C correspond to weak acid sites, medium acid sites, and strong acid sites, respectively. The TiO_2 NP support showed desorption peaks at 120 and 280 °C, whereas the TiO_2 HMS support showed desorption peaks at 80, 310, and 530 °C. Compared with the other supports, the TiO_2 NR support showed desorption peaks at lower temperatures (70, 280, and 530 °C). The total acidity of the TiO_2 supports decreased in the following order: TiO_2 NP

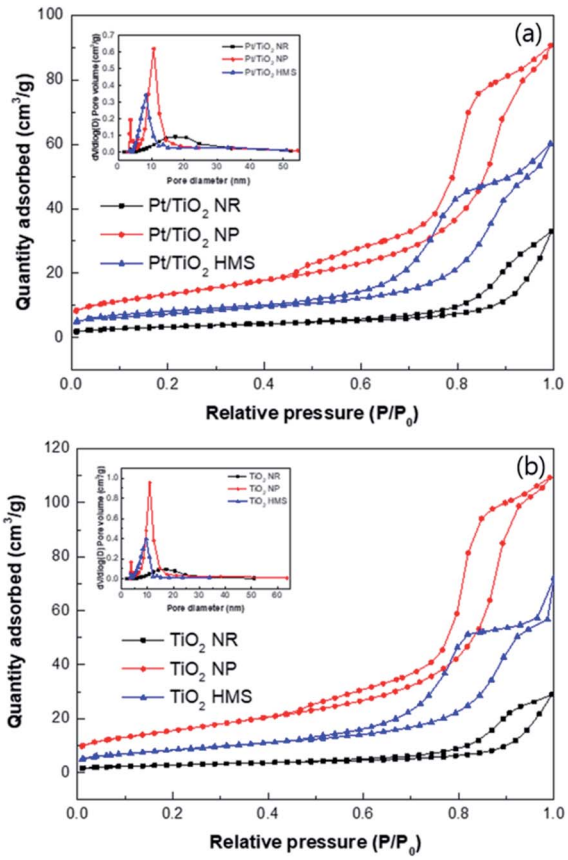

Fig. 1 N_2 isotherm curves and pore size distributions of (a) TiO_2 supports and (b) Pt/TiO_2 catalysts.

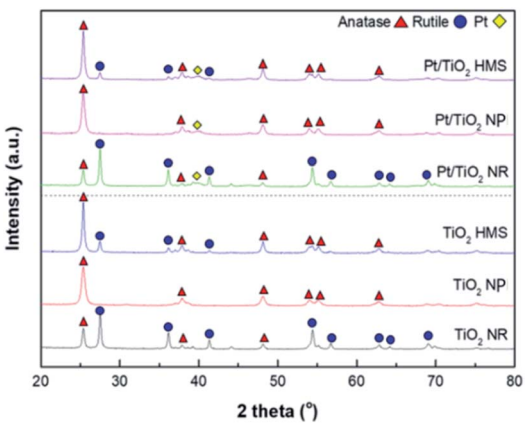

Fig. 2 XRD patterns of TiO_2 supports and Pt/TiO_2 catalysts.

Table 1 Physical and chemical properties of TiO_2 supports and Pt/TiO_2 catalysts

	S_{BET} ($m^2\ g^{-1}$)	V_{Total} ($cm^3\ g^{-1}$)	Pore diameter (nm)	Weight (%)		Acidity (mmol g^{-1})	Binding energy (eV)		Metal dispersion (%)
				Anatase	Rutile		Ti^{4+}	Pt^0	
TiO_2 NR	10	0.04	14.8	31	69	0.10	458.7	—	
TiO_2 NP	56	0.16	9.70	100	—	0.31	458.9	—	
TiO_2 HMS	30	0.08	8.50	79	21	0.27	458.6	—	
Pt/TiO_2 NR	12	0.05	15.7	31	69	0.11	459.1	71.07	9
Pt/TIO_2 NP	48	0.14	9.20	100	—	0.30	459.3	71.20	12
Pt/TiO_2 HMS	27	0.09	9.30	79	21	0.28	459.3	71.20	3

(0.31 mmol g^{-1}) > TiO_2 HMS (0.27 mmol g^{-1}) > TiO_2 NR (0.1 mmol g^{-1}). After Pt loading, similar results were observed.

Fig. 4 shows the H_2-TPR profiles of the TiO_2 supports and Pt/TiO_2 catalysts. The TiO_2 supports showed two reduction peaks around 400–500 and 750 °C, which are corresponded to the reduction of the TiO_2 support.[15,16] The TiO_2 NR exhibited lower reduction temperature than other support, indicating the TiO_2 NR can be more easily formation Ti^{3+} and oxygen vacancies on surface.[17] All the Pt/TiO_2 catalysts showed a reduction peak around 300–500 °C ascribed to the reduction of Pt–TiO_x interface sites by an interaction between Pt and TiO_2.[18] The Pt/TiO_2 HMS catalyst exhibited three reduction peaks around 300, 400, and <500 °C. The first peak is related to the reduction of PtO species weakly interacting with the TiO_2 support,[19] the second peak is related to the reduction of Pt–TiO_x interface sites, and the third peak correspond to the reduction of the surface-capping oxygen on the TiO_2 support.[17,18]

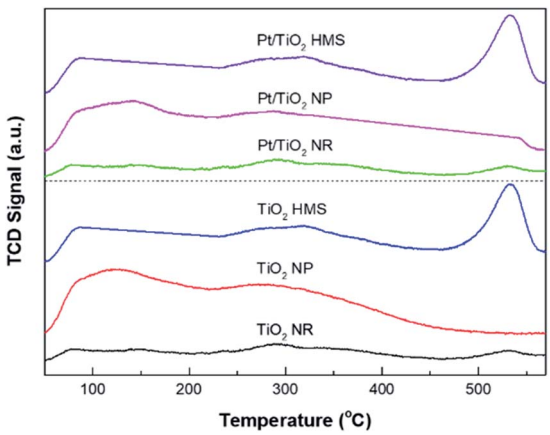

Fig. 3 NH_3-TPD profiles of TiO_2 supports and Pt/TiO_2 catalysts.

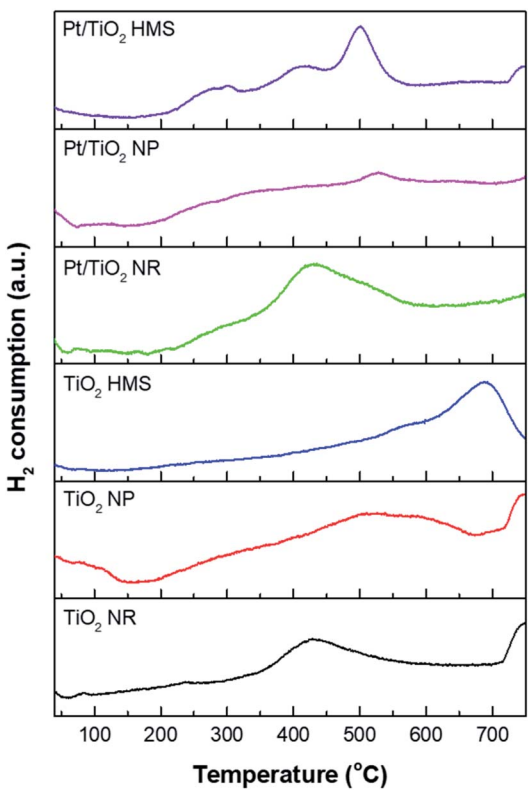

Fig. 4 H_2-TPR profiles of TiO_2 supports and Pt/TiO_2 catalysts.

Fig. 5 exhibits the H_2-TPD profiles for the Pt/TiO_2 catalysts. The desorption temperature is relevant to the adsorption energy of hydrogen and the nature of hydrogen species. For Pt/TiO_2 HMS and Pt/TiO_2 NP catalysts, the double peaks were revealed under 300 °C, indicating hydrogen adsorption on Pt surface.[20] Compared to the Pt/TiO_2 NP catalyst, the Pt/TiO_2 HMS had a large amount of hydrogen adsorbed on Pt due to its 3D structure. The Pt/TiO_2 NR showed double peaks at 74 °C and 535 °C, resulting from hydrogen on Pt and H spillover species, respectively. This H spillover can induce SMSIs owing to the reduction of TiO_2 supports to TiO_x ($x < 2$), leading to improving the catalytic activity and selectivity.[21]

The XPS spectra of the TiO_2 supports and Pt/TiO_2 catalysts in the Ti 2p and Pt 4f regions are shown in Fig. 6 and the results are summarized in Table 1. The TiO_2 supports exhibited two peaks at 458.7 and 464.5 eV corresponding to the Ti $2p_{3/2}$ and Ti $2p_{1/2}$ peaks of Ti^{4+}, respectively.[22] After Pt loading, the Ti 2p peaks shifted toward higher binding energies, which is indicative of an interaction between Pt and TiO_2.[23] The binding energy of the Ti 2p peak for the Pt/TiO_2 NR catalyst was lower than those for the Pt/TiO_2 NP and Pt/TiO_2 HMS catalysts, indicating that Ti^{3+} species exist on the Pt/TiO_2 NR catalyst.[24] As shown in Fig. 6c, two Pt peaks are observed at 71.0 and 74.3 eV corresponding to Pt $4f_{7/2}$ and Pt $4f_{5/2}$, respectively. The Pt $4f_{7/2}$ peak at 71.0 eV corresponds to the metallic state. The binding energies of the Pt $4f_{7/2}$ peaks for the Pt/TiO_2 NR catalyst are slightly lower than those for the Pt/TiO_2 NP and Pt/TiO_2 HMS catalysts. Generally, SMSIs in metal-supported TiO_2 catalysts are introduced during thermal treatment in the range of 150–600 °C under H_2 flow.[25,26] Rui *et al.* reported that an SMSI effect in a Pt/TiO_2 catalyst was produced by chemical reduction using $NaBH_4$ or HCHO solution.[27] Among the prepared Pt/TiO_2

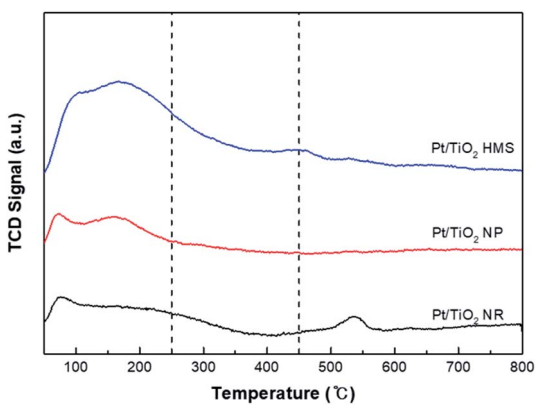

Fig. 5 H_2-TPD profiles of Pt/TiO_2 catalysts.

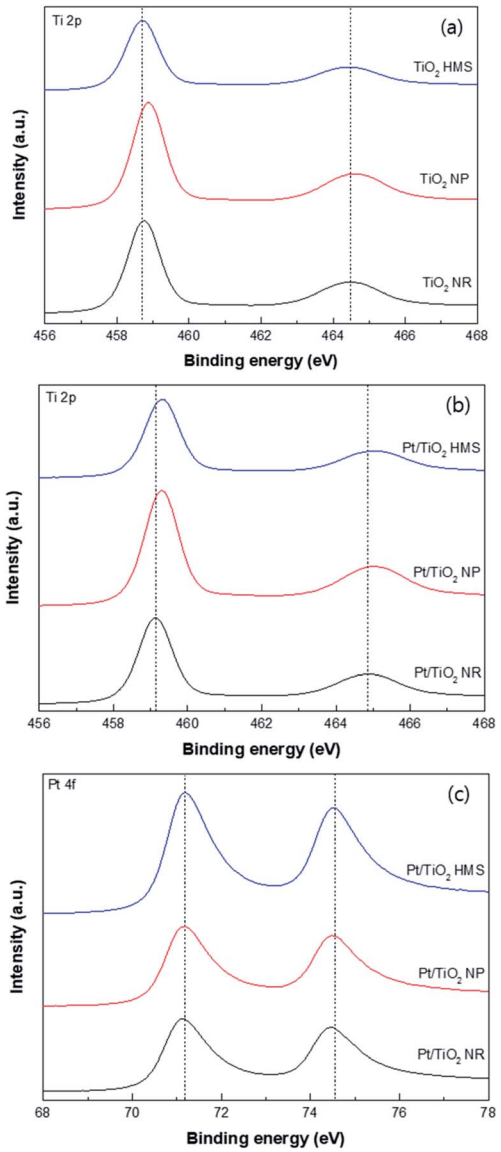

Fig. 6 XPS spectra of TiO_2 supports and Pt/TiO_2 catalysts: (a) Ti 2p of TiO_2, (b) Ti 2p of Pt/TiO_2, and (c) Pt 4f of Pt/TiO_2.

catalysts, the Pt/TiO_2 NR catalyst exhibited a lower binding energy for the peak at 70.18 eV, which was attributed to an SMSI effect.

Fig. 7 shows the FE-SEM images of the TiO_2 supports. The TiO_2 NR support shows linear structures with lengths of 500 nm to 1 μm. The TiO_2 NP support contains NP with sizes of 300–500 nm. The TiO_2 HMS support shows HMS with sizes of 3–5 μm. Fig. 8 shows representative FE-TEM images and particle size distribution of the Pt/TiO_2 catalysts. The average particle size was measured using 200 spherical Pt NP. The average particle size in the Pt/TiO_2 catalysts increased in the order Pt/TiO_2 NP (4.52 nm) < Pt/TiO_2 NR (5.25 nm) < Pt/TiO_2 HMS (6.48 nm). The dispersion of Pt in the Pt/TiO_2 catalysts was estimated by CO chemisorption (Table 1). The Pt/TiO_2 NP catalyst exhibited the highest Pt dispersion of 12%, whereas the Pt/TiO_2 HMS catalyst exhibited the lowest Pt dispersion of 3%. These results correspond to the FE-TEM results.

3.2. Hydrogenation of furfural

The catalytic activities of the prepared TiO_2 supports and Pt/TiO_2 catalysts were investigated with respect to the hydrogenation of furfural under 20 bar of H_2 at 170 °C for 2 h; the results are summarized in Table 2. Furfural hydrogenation did not proceed to any significant extent over the TiO_2 supports alone. The conversion of furfural decreased with Pt dispersion in the order Pt/TiO_2 NP > Pt/TiO_2 NR > Pt/TiO_2 HMS. However, the Pt/TiO_2 NR catalyst exhibited the highest CPO selectivity of 35.2%. The selectivity for CPO can be affected by several factors such as support properties, hydrogen pressure, and solvent effects. Firstly, the catalytic activities were affected by TiO_2 properties. The Pt/TiO_2 NP with 0D structure revealed the highest conversion of furfural due to the largest specific surface area. Although the Pt/TiO_2 HMS had 3D structure to facilitate hydrogen adsorption, the lowest conversion and selectivity were obtained. This is ascribed to a large quantity of strong acid sites, which causes polymerization and lowers the

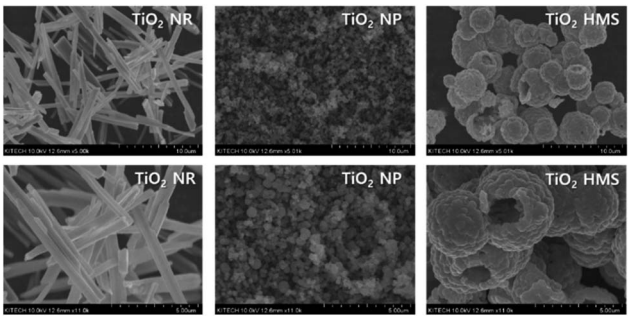

Fig. 7 FE-SEM images of TiO_2 supports.

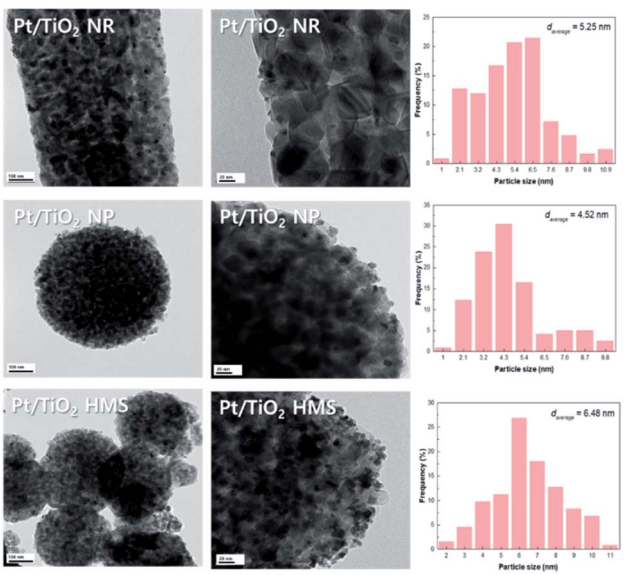

Fig. 8 FE-TEM images of Pt/TiO_2 catalysts.

Table 2 Hydrogenation of furfural over TiO_2 supports and Pt/TiO_2 catalysts[a]

	Conversion (%)	Selectivity (%)				
		FA	THFAL	CPO	CPL	Others
TiO_2 NR	0.3	—	—	—	—	100
TiO_2 NP	1.2	—	—	—	—	100
TiO_2 HMS	0.3	—	—	—	—	100
Pt/TiO_2 NR	90	2.3	1.5	35.2	—	61
Pt/TIO_2 NP	96	2.0	—	13.6	1.8	82.6
Pt/TiO_2 HMS	78	4.0	—	14.2	—	81.8

[a] Reaction conditions: P_{H2} = 20 bar, reaction temp. = 170 °C, and reaction time = 2 h.

catalytic activity.[28,29] In contrast, the Pt/TiO_2 NR (1D) showed the highest CPO selectivity regardless of Pt dispersion and specific surface area. We suggested that the large pore size of Pt/TiO_2 NR catalyst can easily access furfural molecules to inside the catalyst pore with minimized steric hindrance.[30] In addition, furfural and FA can be converted into polymers by heat treatment or acid sites.[31,32] Based on the NH_3-TPD results, the Pt/TiO_2 NR catalyst has the lowest total acidity and thus can produce more CPO by rearrangement. Cyclopentanol (CPL), THFAL, and other non-identified materials were detected as byproducts.

The effect of reaction time on furfural hydrogenation over the Pt/TiO_2 catalysts was investigated under at 170 °C, P_{H2} = 20 bar, and reaction time in the range of 30 min to 240 min (Fig. 9). As the reaction time increased, the furfural conversion gradually increased. With the Pt/TiO_2 NP catalyst, a furfural conversion of 99.8% was achieved at 170 °C for 3 h. This catalyst exhibited the highest catalytic activity due to its high Pt dispersion. Interestingly, the Pt/TiO_2 NP catalyst showed higher CPO selectivity than the Pt/TiO_2 HMS catalyst despite having a higher total acidity, likely because the Pt/TiO_2 NP catalyst mainly contained weak acid sites, whereas strong acid sites were predominant on the Pt/TiO_2 HMS catalyst. Although the Pt/TiO_2 NP catalyst had higher acidity than the Pt/TiO_2 NR catalyst, the acid site distribution was dominant in weak acid sites compared to Pt/TiO_2 HMS. The Pt/TiO_2 NP catalyst exhibited high CPO selectivity. We suggested that selectivity of product affected by two perspective; SMSI effect and hydrogen adsorption strength. Based on the XPS and H_2-TPD results, the SMSI effect was occurred over Pt/TiO_2 NR catalyst. The SMSI effect induced by H spillover species during the reduction process with $NaBH_4$ solution. The H spillover species on Pt surface can diffuse into TiO_2 NR and reduce TiO_2 surface, resulting in the formation of Pt covered from TiO_x and oxygen vacancy. The covered Pt particles from TiO_x affect the adsorption strength of H_2, resulting higher CPO yield with retarding over-hydrogenation or polymerization. The C=O (carbonyl) group in furfural adsorbs selectively on the oxygen vacancies and is hydrogenated with the H spillover species.[33–36]

Based on the XPS results, the Ti 2p and Pt 4f binding energies of the Pt/TiO_2 NR catalyst in Ti 2p and Pt 4f are lower than

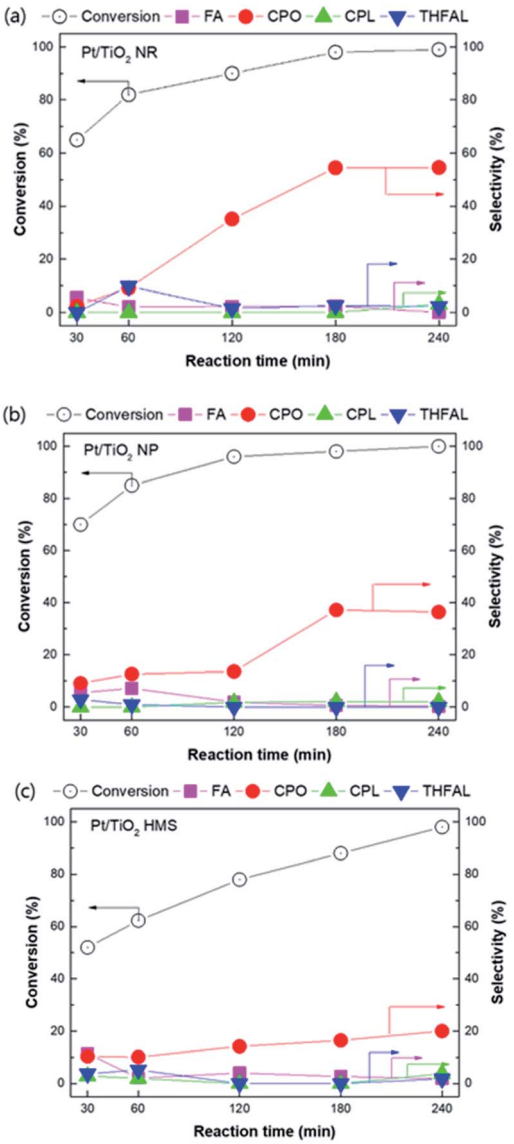

Fig. 9 Furfural hydrogenation over (a) Pt/TiO_2 NR, (b) Pt/TiO_2 NP, and (c) Pt/TiO_2 HMS catalysts.

those of the other catalysts. Riyapan *et al.* reported that electron charge transfer from Ti species to Pd affects the adsorption strength of ethylene on the Pd surface, resulting in high selectivity for ethylene.[37] Lee *et al.* reported that the interaction between TiO_y species generated at various temperatures and Co NPs provides bifunctional sites for the selective hydrogenation of furfural by controlling the SMSI effect.[38] As the reaction time increased, the CPO selectivity gradually increased over the Pt/TiO_2 NR and Pt/TiO_2 NP catalysts. However, only a slight increase in the CPO selectivity occurred over the Pt/TiO_2 HMS catalyst. Although Pt/TiO_2 NR exhibited SMSI effect, we considered the effect of TiO_2 phase. Aschauer *et al.* reported that oxygen vacancies in reduced anatase phase of TiO_2 has favorable adsorption site for H_2 atoms.[39] Islam *et al.* reported that molecular of H_2 cannot easily interaction with rutile phase of TiO_2 support.[40] From the XRD results, the Pt/TiO_2 NR catalyst

exhibited higher amount of rutile phase than other catalysts. We suggest that the SMSI effect and hydrogen adsorption strength may affect CPO selectivity in furfural hydrogenation. Furfural hydrogenation involves various reaction pathways, including C=C and C=O hydrogenation, hydrogenolysis, and rearrangement to produce various materials such as FA, CPO, CPL, 2-methylfuran, *n*-butanol, and 2-pentanol. The Pt/TiO_2 NR catalyst showed the highest catalytic performance in the selective hydrogenation of furfural to CPO. Thus, electron charge transfer from Ti species to Pt in the Pt/TiO_2 NR catalyst having high content of rutile phase may affect the selectivity for these products by controlling the adsorption strength between the reactant and the Pt surface, which can retard the formation of byproducts (Fig. 10).

The effect of reaction temperature on furfural hydrogenation over the Pt/TiO_2 NR catalyst was investigated under at $P_{H2} = 20$ bar for 3 h at reaction temperature in the range of 110–190 °C (Fig. 11). Furfural conversion increased with increasing reaction temperature. In the range of 110–130 °C, FA was predominantly produced and FA selectivity increased from 72.2% to 84.1%. However, at reaction temperatures over 130 °C, FA selectivity dramatically decreased with a concomitant increase in CPO selectivity. At high temperatures, the rearrangement of FA into 4-hydroxy-2-cyclopentanone (HCP) is promoted by H^+ ions in the aqueous phase.[41,42] The produced HCP can be converted into CPO by further hydrogenation. At higher temperatures, more H^+ ions are generated, thereby increasing CPO selectivity. However, as the reaction temperature increased from 170 to 190 °C, CPO selectivity was dramatically decreased to 0% owing to the formation of oligomers at high temperatures.[43,44]

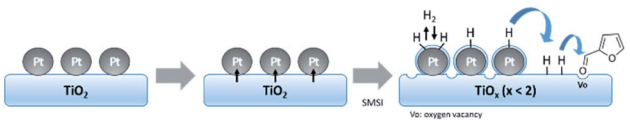

Fig. 10 Illustration of the SMSI effect in the Pt/TiO_2 NR catalyst.

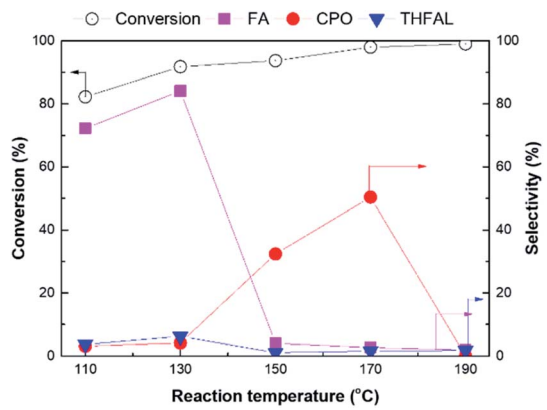

Fig. 11 Effect of reaction temperature of furfural hydrogenation over the Pt/TiO_2 NR catalyst.

4. Conclusions

Pt/TiO_2 NR, NP, and HMS catalysts were prepared by the impregnation–chemical reduction method for the selective hydrogenation of furfural to CPO. Although furfural conversion increased with Pt dispersion, CPO selectivity was strongly affected by TiO_2 properties and the SMSI effect. The Pt/TiO_2 HMS catalyst, which had the highest acidity, exhibited the lowest CPO selectivity at reaction times from 30 to 240 min owing to polymerization. The Pt/TiO_2 NP catalyst had predominant weak acid sites and higher total acidity than Pt/TiO_2 NR, resulting in lower CPO selectivity than Pt/TiO_2 NR. We suggested that two perspective on the TiO_2 properties effect and SMSI effect. Among three different supports, the Pt/TiO_2 NR with the largest pore size facilitated the furfural molecules inside the catalyst and minimized the steric hindrance between the reactant and catalyst, enhancing the CPO selectivity. Based on the XPS results, an SMSI effect was observed after Pt loading on the TiO_2 NR support. Electron charge transfer from Ti species to Pt in the Pt/TiO_2 NR catalyst may control the adsorption strength between the reactant and the Pt surface, resulting in higher CPO selectivity over the Pt/TiO_2 NR catalyst than over the Pt/TiO_2 NP catalyst. The Pt/TiO_2 NR catalyst showed highest catalytic activity for 98% furfural conversion and 50.4% CPO selectivity.

Conflicts of interest

There are no conflicts to declare.

Author contributions

Mi Yeon Byun: conceptualization, methodology, investigation, writing – original draft. Ye Eun Kim: investigation, data curation, visualization, Jae Ho Baek: visualization, Jungho Jae: supervision, Man Sig Lee: writing – review & editing, supervision.

Acknowledgements

This work was supported by the Korea Institute of Industrial Technology through Research and Development (EH210006, EO210001), and Ulsan Metropolitan City (IZ210064).

Notes and references

1 X. Wang, Z. Li, J. Shi and Y. Yu, One-Dimensional Titanium Dioxide Nanomaterials: Nanowires, Nanorods, and Nanobelt, *Chem. Rev.*, 2014, **114**, 9346–9384.
2 C. Tian, H. Fang, H. Chen, W. Chen, S. Zhou, X. Duan, X. Liu and Y. Yuan, Photodeposition of Pd onto TiO_2 nanowires for aqueous-phase selective hydrogenation of phenolics to cyclohexanones, *Nanoscale*, 2020, **12**, 2603–2612.
3 H. Song, Z. Liu, Y. Wang, N. Zhang, X. Qu, K. Guo, M. Xiao and H. Gai, Template-free synthesis of hollow TiO_2 nanospheres supported Pt for selective photocatalytic

oxidation of benzyl alcohol to benzaldehyde, *Green Energy Environ.*, 2019, **4**(3), 278–286.
4 G. K. Alqurashi, A. Al-Shehri and K. Narasimharao, Effect of TiO_2 morphology on the benzyl alcohol oxidation activity of Fe_2O_3-TiO_2 nanomaterials, *RSC Adv.*, 2016, **6**, 71076–71091.
5 M. Hronec, K. Fulajtárová, I. Vávra, T. Soták, E. Dobročka and M. Mičušík, Carbon supported Pd-Cu catalysts for highly selective rearrangement of furfural to cyclopentanone, *Appl. Catal., B*, 2016, **181**, 210–219.
6 J. Wu, G. Gao, J. Li, P. Sun, X. Long and F. Li, Efficient and versatile CuNi alloy nanocatalysts for the highly selective hydrogenation of furfural, *Appl. Catal., B*, 2017, **203**, 227–236.
7 M. Y. Byun, D. Park and M. S. Lee, Effect of oxide supports on the activity of Pd based catalysts for furfural hydrogenation, *Catalysts*, 2020, **10**, 837.
8 V. V. Ordomsky, J. c. Schouten, J. Van Der Schaaf and T. A. Nijhuis, Biphasic single-reactor process for dehydration of xylose and hydrogenation of produced furfural, *Appl. Catal., A*, 2013, **451**, 6–13.
9 Y. Wang, X. Jiang and Y. Xia, A solution-phase, precursor route to polycrystalline SnO_2 nanowires that can be used for gas sensing under ambient conditions, *J. Am. Chem. Soc.*, 2003, **125**, 16176–16177.
10 S. Lee, G. Sang, J. Lee, J. Lee and H. Suk, Mesoporous TiO_2 nanowires as bi-functional materials for dye-sensitized solar cells, *Electrochim. Acta*, 2012, **74**, 83–86.
11 G. Cheng, M. S. Akhtar, O. B. Yang and F. J. Stadler, Structure modification fo anatase TiO_2 nanomaterials-based photoanodes for efficient dye-sensitized solar cells, *Electrochim. Acta*, 2013, **113**, 527–535.
12 T. Z. Ren, Z. Y. Yuan and B. L. Su, Surfactant-assisted preparation of hollow microspheres of mesoporous TiO_2, *Chem. Phys. Lett.*, 2003, **374**, 170–175.
13 H. Huang and D. Y. C. Leung, Complete oxidation of formaldehyde at room temperature using TiO_2 supported metallic Pd nanoparticles, *ACS Catal.*, 2011, **1**, 348–354.
14 R. A. Spurr and H. Myers, Quantitative analysis of anatase-rutile mixtures with an X-ray diffractometer, *Anal. Chem.*, 1957, **29**, 760–762.
15 V. Bratan, C. Munteanu, C. Hornoiu, A. Vasile, F. Papa, R. State, S. Preda, D. Culita and N. I. Ionescu, CO oxidation over Pd supported catalysts-In situ study of the electric and catalytic properties, *Appl. Catal., B*, 2017, **207**, 166–173.
16 K. Czupryn, I. Kocemba and J. Rynkowski, Photocatalytic CO oxidation with water over Pt/TiO_2 catalysts, *React. Kinet., Mech. Catal.*, 2018, **124**, 187–201.
17 T. Ekou, L. Ekou, A. Vicente, G. Lafaye, S. Pronier, C. Especel and P. Marécot, Citral hydrogenation over Rh and Pt catalysts supported on TiO_2: influence of the preparation and activation protocols of the catalysts, *J. Mol. Catal. A: Chem.*, 2011, **337**, 82–88.
18 S. Pisduangdaw, O. Mekasuwandumrong, H. Yoshida, S. I. Fujita, M. Arai and J. Panpranot, Flame-made Pt/TiO_2 catalysts for the liquid-phase selective hydrogenation of 3-nitrostyrene, *Appl. Catal., A*, 2015, **490**, 193–200.
19 S. Bhogeswararao and D. Srinivas, Catalytic conversion of furfural to industrial chemicals over supported Pt and Pd catalysts, *J. Catal.*, 2015, **327**, 65–77.
20 J. T. Miller, B. L. Meyers, F. S. Modica, G. S. Lane, M. Vaarkamp and D. C. Koningsberger, Hydrogen temperature-programmed desorption (H_2 TPD) of supported platinum catalysts, *J. Catal.*, 1993, **143**, 395–408.
21 W. C. Conner and J. L. Falconer, Spillover in heterogeneous catalysis, *Chem. Rev.*, 1995, **95**, 759–768.
22 J. Liqiang, F. Honggang, W. Baiqi, W. Dejun, X. Baifu, L. Shudan and S. Jiazhong, Effects of Sn dopant on the photoinduced charge property and photocatalytic activity of TiO_2 nanoparticles, *Appl. Catal., B*, 2006, **62**, 282–291.
23 L. Yu, Y. Shao and D. Li, Direct combination of hydrogen evolution from water and methane conversion in a photocatalytic system over Pt/TiO_2, *Appl. Catal., B*, 2017, **204**, 216–223.
24 X. Yao, L. Chen, J. Cao, F. Yang, W. Tan and L. Dong, Morphology and crystal-plane effects of CeO_2 on TiO_2/CeO_2 catalysts during NH_3-SCR reaction, *Ind. Eng. Chem. Res.*, 2018, **57**, 12407–12419.
25 R. T. K. Baker, E. B. Prestridge and L. L. Murrell, Electron microscopy of supported metal particles. III. The role of the metal in an SMSI interaction, *J. Catal.*, 1983, **79**, 348–358.
26 H. Huang, D. Y. C. Leung and D. Ye, Effect of reduction treatment on structural properties of TiO_2 supported Pt nanoparticles and their catalytic activity for formaldehyde oxidation, *J. Mater. Chem.*, 2011, **21**, 9647–9652.
27 Z. Rui, L. Chen, H. Chen and H. Ji, Strong metal-support interaction in Pt/TiO_2 induced by mild HCHO and $NaBH_4$ solution reduction and its effect on catalytic toluene combustion, *Ind. Eng. Chem. Res.*, 2014, **53**, 15879–15888.
28 T. D. Swift, H. Nguyen, Z. Erdman, J. S. Kruger, V. Nikolakis and D. G. Vlachos, Tandem Lewis acid/Brønsted acid-catalyzed conversion of carbohydrates to 5-hydroxymethylfurfural using zeolite beta, *J. Catal.*, 2016, **333**, 149–161.
29 C. Wang, Z. Yu, Y. Yang, Z. Sun, Y. Wang, C. Shi, Y.-Y. Liu, A. Wang, K. Leus and P. V. D. Voort, Hydrogenative ring-rearrangement of furfural to cyclopentanone over Pd/UiO-66-NO_2 with tunable missing-linker defects, *Molecules*, 2021, **26**, 5736.
30 Z. Yu, L. Zhang, Z. Zhang, S. Zhang, S. Hu, J. Xiang, Y. Wang, Q. Liu, Q. Liu and X. Hu, Silica of varied pore sizes as supports of copper catalysts for hydrogenation of furfural and phenolics: impact of steric hindrance, *Int. J. Hydrogen Energy*, 2020, **45**, 2720–2728.
31 M. Hronec and K. Fulajtarová, Selective transformation of furfural to cyclopentanone, *Catal. Commun.*, 2012, **24**, 100–104.
32 T. Kim, R. S. Assary, R. E. Pauls, C. L. Marshall, L. A. Curtiss and P. C. Stair, Thermodynamics and reaction pathways of furfural alcohol oligomer formation, *Catal. Commun.*, 2014, **46**, 66–70.
33 R. Gao, X. Li, L. Guo, Z. Tong, Q. Deng, J. Wang, Z. Zeng, J.-J. Zou and S. Deng, Pyrochlore/Al_2O_3 composites supported Pd for the selective synthesis of

cyclopentanones from biobased furfurals, *Appl. Catal., A*, 2021, **612**, 117985.
34 Q. Deng, R. Gao, X. Li, J. Wang, Z. Zeng, J.-J. Zou and S. Deng, Hydrogenative ring-rearrangement of biobased furanic aldehydes to cyclopentanone compounds over Pd/pyrochlore by introducing oxygen vacancies, *ACS Catal.*, 2020, **10**, 7355–7366.
35 Z. Tong, R. Gao, X. Li, L. Guo, J. Wang, Z. Zeng, Q. Deng and S. Deng, Highly controllable hydrogenative ring rearrangement and complete hydrogenation of biobased furfurals over Pd/$La_2B_2O_7$ (B = Ti, Zr, Ce), *ChemCatChem*, 2021, **13**, 4549–4556.
36 T. W. van Deelen, C. H. Mejia and K. P. de Jong, Control of metal-support interactions in heterogeneous catalysts to enhance activity and selectivity, *Nat. Catal.*, 2019, **2**, 955–970.
37 S. Riyapan, Y. Boonyongmaneerat, O. Mekasuwandumrong, P. Praserthdam and J. Panpranot, Effect of surface Ti^{3+} on the sol-gel derived TiO_2 in the selective acetylene hydrogenation on Pd/TiO_2 catalysts, *Catal. Today*, 2015, **245**, 134–138.
38 J. Lee, S. P. Burt, C. A. Carrero, A. C. Alba-Rubio, I. Ro, B. J. O'Neill, H. J. Kim, D. H. K. Jackson, T. F. Kuech, I. Hermans, J. A. Dumesic and G. W. Huber, Stabilizing cobalt catalysts for aqueous-phase reactions by strong metal-support interaction, *J. Catal.*, 2015, **330**, 19–27.
39 U. Aschauer and A. Selloni, Hydrogen interaction with the anatase TiO_2(101) surface, *Phys. Chem. Chem. Phys.*, 2012, **14**, 16595–16602.
40 M. M. Islam, M. Calatayud and G. Pacchioni, Hydrogen adsorption and diffusion on the anatase TiO_2(101) surface: a first-principles investigation, *J. Phys. Chem. C*, 2011, **115**, 6809–6814.
41 M. Hronec, K. Fulajtárova and T. Soták, Highly selective rearrangement of furfuryl alcohol to cyclopentanone, *Appl. Catal., B*, 2014, **154–155**, 294–300.
42 M. Kronec, K. Fulajtarova and T. Sotak, Kinetics of high temperature conversion of furfuryl alcohol in water, *J. Ind. Eng. Chem.*, 2014, **20**, 650–655.
43 Y.-F. Ma, H. Wang, G.-Y. Xu, X.-H. Liu, Y. Zhang and Y. Fu, Selective conversion of furfural to cyclopentanol over cobalt catalysts in one step, *Chin. Chem. Lett.*, 2017, **28**, 1153–1158.
44 Y. Li, X. Guo, D. Liu, X. Mu, X. Chen and Y. Shi, Selective conversion of furfural to cyclopentanone or cyclopentanol using Co-Ni catalyst in water, *Catalysts*, 2018, **8**, 193.